ISSN 1070-3284, Russian Journal of Coordination Chemistry, 2018, Vol. 44, No. 10, pp. 626–634. © Pleiades Publishing, Ltd., 2018.
Original Russian Text © G.K. Fukin, M.A. Samsonov, E.V. Baranov, A.V. Cherkasov, R.V. Rumyantsev, A.V. Arapova, 2018, published in Koordinatsionnaya Khimiya, 2018, Vol. 44, No. 5, pp. 325–332.

Electron Density Distribution and Structural and Energy Aspects of the Phase Transition in the Crystals of the Triphenylantimony Dimethacrylate Complex

G. K. Fukin[a], *, M. A. Samsonov[a], E. V. Baranov[a], A. V. Cherkasov[a], R. V. Rumyantsev[a], and A. V. Arapova[a]

[a] *Razuvaev Institute of Organometallic Chemistry, Russian Academy of Sciences, Nizhny Novgorod, 603950 Russia*

**e-mail: gera@iomc.ras.ru*

Received December 29, 2017

Abstract—The electron density distribution in $Ph_3Sb(O_2CC(Me)=CH_2)_2 \cdot C_6H_6$ and structural and energy aspects of the phase transition in the crystals of this compound were investigated using a series of common (**Ib**–**Ie**) and high-precision (**Ia**) X-ray diffraction experiments. A considerable difference between the root-mean-square atomic displacements in two chemically equivalent methyl groups of the methacrylate ligands was revealed. This difference was shown to be caused by considerable energy difference of the intra- and intermolecular contacts of the corresponding methyl groups.

Keywords: triphenylantimony methacrylate complex, high-precision X-ray diffraction, phase transition, Bader's theory Atoms in Molecules, root-mean-square atomic displacements

DOI: 10.1134/S1070328418100020

INTRODUCTION

The triarylantimony(V) carboxylate complexes ($Ar_3Sb(O_2CR)_2$) possess a broad spectrum of applications. Some triarylantimony(V) dicarboxylates are being tested for antitumor, apoptotic, and cytotoxic activities [1–7]. Some complexes of this class are applied in organic synthesis as reagents and catalysts [8–11]. Furthermore, polymeric photosensitive materials based on triphenylantimony dicarboxylate complexes have recently been developed [12]. Our interest in the complex $Ph_3Sb(O_2CC(Me)=CH_2)_2$ [13] is related to the search for structural and energy parameters of phase transition in this compound [14]. This publication describes high-precision calorimetric studies of the triphenylantimony(V) dimethacrylate complex. During the measurements, a low-temperature anomaly was detected in the temperature dependence of the heat capacity, which was reproduced every time as the compound was cooled and then heated again (Fig. 1). The authors suggested that this anomaly was of structural nature and could be associated with excitation of vibrations of some atomic groups on heating and arrest of these vibrations on cooling. In terms of Westrum–McCullough thermodynamic classification [15], the observed phase transition refers to the equilibrium relaxation order $\rightleftarrows$ disorder λ-transition.

EXPERIMENTAL

The triarylantimony(V) dimethacrylate complex, $Ph_3Sb(O_2CC(Me)=CH_2)_2 \cdot C_6H_6$ (**I**), was prepared by a known procedure described in [13].

The X-ray diffraction study of $Ph_3Sb(O_2CC(Me)=CH_2)_2 \cdot C_6H_6$ was carried out at 100 (**Ib**), 145 (**Ic**), 158 (**Id**), and 170 K (**Ie**) on a Bruker D8 QUEST automated diffractometer (CMOS detector). The high-precision X-ray diffraction study of complex **Ia** and the study of polymorph **II** at 100 K were performed on an Oxford Xcalibur (Eos detector) diffractometer (graphite monochromators, MoK_α radiation, λ = 0.71073 Å). The experimental sets of reflection intensities were integrated using Saint [16] and CrysAlisPro [17] software. The SADABS [18] and SCALE3 ABSPACK [19] programs were used to apply absorption corrections. The structures were solved by direct methods and refined by full-matrix least-squares calculations on F^2 using the SHELXTL program [20]. All non-hydrogen atoms were refined in the anisotropic approximation. The hydrogen atoms were placed into geometrically calculated positions and refined in the riding model.

The multipole refinement for complex **Ia** was carried out with the Hansen–Coppens model [21] using a MoPro program package [22]. All hydrogen atoms in high-precision X-ray diffraction study were normal-

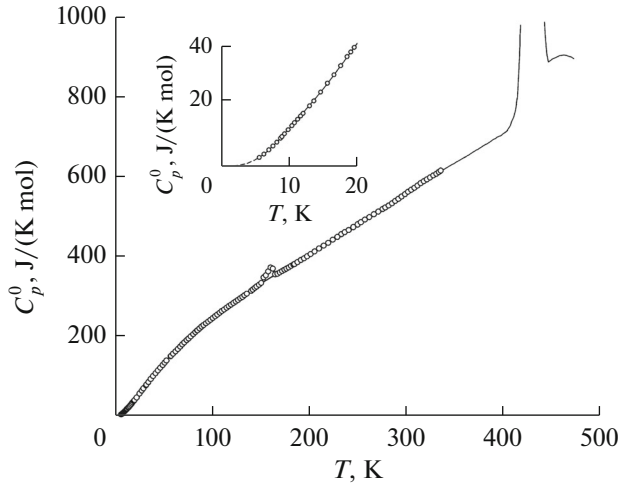

Fig. 1. Temperature dependence of the heat capacity of triphenylantimony dimethacrylate [14].

ized, prior to the multipole refinement, to ideal neutron diffraction distances [23]. The expansion level was hexadecapole for antimony, octapole for all non-hydrogen atoms, and dipole for hydrogen atoms. All bonded pairs of atoms met the Hirshfeld test [24]. The topological analysis of the experimental function $\rho(\mathbf{r})$ was carried out by means of WINXPRO program package [25].

The key crystallographic data and X-ray diffraction experiment parameters for **Ia**–**Ie** and **II** are summarized in Table 1.

The structures are deposited with the Cambridge Crystallographic Centre (nos. 1813825 (**Ia**; model of non-interacting atoms), 1813826 (**Ia**; multipole model), 1813827 (**Ib**), 1813828 (**Ic**), 1813829 (**Id**), 1813830 (**Ie**), 1813831 (**II**); deposit@ccdc.cam.ac.uk or http://www.ccdc.cam.ac.uk/data_request/cif).

The heat capacity of the sample in the 130–500 K range was measured using a DSC204F1 Phoenix differential scanning calorimeter (NetzschGerätebau, Germany). The design of DSC204F1 calorimeter and the procedure of measurements were reported in [26, 27]. The operation reliability of the calorimeter was checked by standard calibration experiments by measuring the thermodynamic characteristics of melting for cyclohexane, mercury, indium, tin, lead, bismuth, and zinc. The sample heating rate was 5 K/min and the nitrogen supply rate was 20 mL/min.

RESULTS AND DISCUSSION

To make sure that the crystals of **Ia**–**Ie** do undergo a phase transition, as in [14], we carried out a differential scanning calorimetry (DSC) study. The DSC curve shows a reproducible endothermic transformation at 155–160 K, related to the phase transition. In the 360–385 K range, irreversible endothermic transformation takes place related to removal of the solvent from the crystal lattice. Further heating leads to endotherm at 418–443 K, associated with melting.

The electron density distribution in the crystals of complex **Ia** was studied by high-precision X-ray diffraction. As for most triarylantimony dicarboxylate complexes [28–30], the Sb atom in **Ia** has a distorted tetragonal pyramidal geometry with *cis*-arranged carboxylate ligands (Fig. 2). Since the geometric parameters of **Ia** are close to those of the previously studied complex [13], here we focus the attention on the topological characteristics of electron density distribution in **Ia**. The deformation electron density (DED) distribution in **Ia** (Fig. 3) is similar to that in the triphenylantimony dicarboxylate complexes we studied [31, 32]. R. Bader's theory was used to investigate the nature of chemical bonds in **Ia** [33]. According to this theory (Table 2), the Sb(1)–O(1,3) and Sb(1)–C(15) bonds in **Ia** are classified as intermediate interactions ($\nabla^2\rho(\mathbf{r}) > 0$, $h_e(\mathbf{r}) < 0$), while the Sb(1)–C(9) and Sb(1)–C(21) bonds are shared interactions ($\nabla^2\rho(\mathbf{r}) < 0$, $h_e(\mathbf{r}) < 0$). Note that in the previously studied triphenylantimony dicarboxylate complexes [31, 32], all Sb–C(Ph) bonds were intermediate type interactions ($\nabla^2\rho(\mathbf{r}) > 0$, $h_e(\mathbf{r}) < 0$). Analysis of the topological characteristics for the Sb(1)–C(9) and Sb(1)–C(21) bonds indicate that the $\nabla^2\rho(\mathbf{r})$ value for the Sb(1)–C(9) bond and the $h_e(\mathbf{r})$ value for the Sb(1)–C(21) bond are close to zero. This suggests that the $\nabla^2\rho(\mathbf{r})$ and $h_e(\mathbf{r})$ values can change the sign, depending on the details of absorption corrections, multipole refinement, and the crystal quality; this may change the R. Bader's type of contacts between the Sb(1), C(9), and C(21) atoms.

Table 1. Key crystallographic characteristics and X-ray experiment details for complexes **I** and **II**

Parameter	Value					
	Ia*	**Ib**	**Ic**	**Id**	**Ie**	**II**
Molecular formula	$C_{29}H_{28}O_4Sb$	$C_{29}H_{28}O_4Sb$	$C_{29}H_{28}O_4Sb$	$C_{29}H_{28}O_4Sb$	$C_{29}H_{28}O_4Sb$	$C_{26}H_{25}O_4Sb$
M	562.26	562.26	562.26	562.26	562.26	523.21
T, K	100(2)	100(2)	145(2)	158(2)	170(2)	100(2)
System	Triclinic	Triclinic	Triclinic	Triclinic	Triclinic	Triclinic
Space group	$P\bar{1}$	$P\bar{1}$	$P\bar{1}$	$P\bar{1}$	$P\bar{1}$	$P\bar{1}$
a, Å	9.25155(3)	9.25155(3)	9.2793(5)	9.2825(5)	9.258(4)	12.0934(3)
b, Å	9.31334(4)	9.31334(4)	9.3426(5)	9.3484(5)	9.260(4)	13.0724(3)
c, Å	14.85770(5)	14.85770(5)	14.9100(8)	14.9225(8)	14.890(6)	14.8849(4)
α, deg	77.4191(3)	77.4191(3)	77.3845(10)	77.3615(10)	77.301(5)	96.550(2)
β, deg	89.8303(2)	89.8303(2)	89.7549(10)	89.7608(10)	89.720(5)	91.989(2)
γ, deg	89.0585(3)	89.0585(3)	88.9200(10)	88.9228(10)	88.971(6)	91.817(2)
V, Å^3	1249.276(8)	1249.276(8)	1261.16(12)	1263.32(12)	1245.1(8)	2334.87(10)
Z	2	2	2	2	2	4
ρ(calcd.), g cm^{-3}	1.495	1.495	1.481	1.478	1.500	1.488
μ, mm^{-1}	1.137	1.137	1.126	1.124	1.141	1.210
F(000)	570	570	570	570	570	1056
Crystal size, mm	0.40 × 0.30 × 0.30	0.40 × 0.30 × 0.30	0.38 × 0.36 × 0.16	0.38 × 0.36 × 0.16	0.38 × 0.36 × 0.16	0.30 × 0.20 × 0.20
θ Range, deg	3.117–55.630	3.117–25.996	3.559–26.000	3.557–25.993	2.608–25.997	3.011–26.000
Number of reflections collected/unique	365282/32710	75355/4924	11772/4792	11810/4794	9242/4780	33433/9122
R_1/wR_2 ($I > 2\sigma(I)$)	0.0244/0.0599	0.0173/0.0467	0.0218/0.0582	0.0215/0.0569	0.0406/0.1087	0.0490/0.1019
GOOF	1.077	1.057	1.095	1.084	1.076	1.050
Residual electron density, e Å^{-3}	2.637/–1.356	0.632/–0.694	0.548/–0.732	0.539/–0.675	1.325/–0.895	0.980/–1.956

* Model of non-interacting atoms.

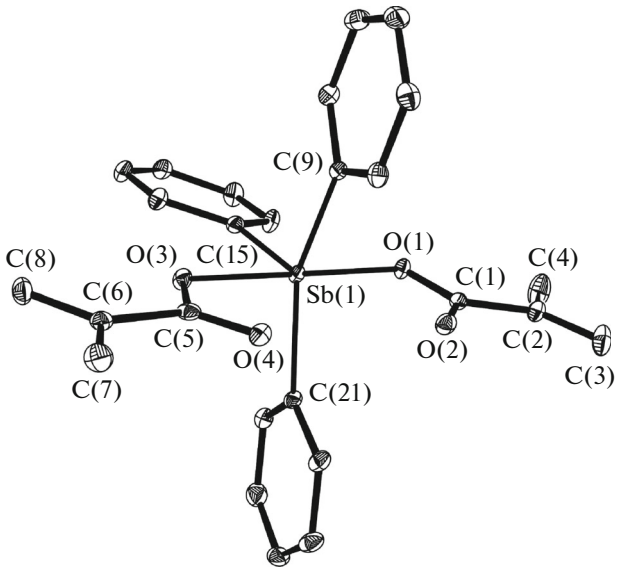

Fig. 2. Molecular structure of $Ph_3Sb(O_2CC(Me)=CH_2)_2$ (**Ia**). The benzene solvation molecule and hydrogen atoms are omitted. The thermal ellipsoids are given at 30% probability level.

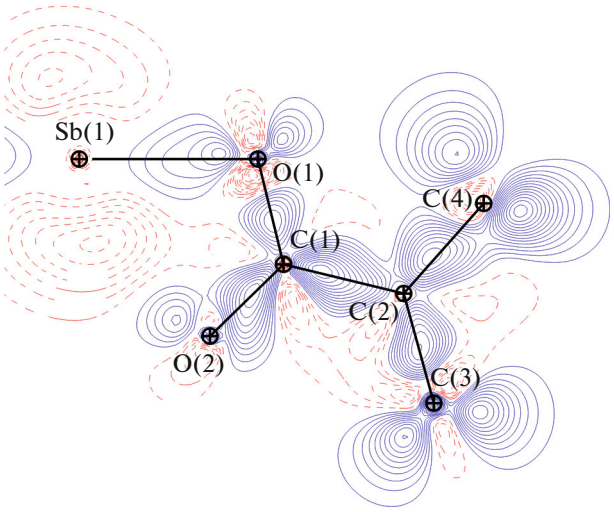

Fig. 3. Experimental deformation electron density distribution in the methacrylate ligand plane. The hydrogen atoms are omitted. The continuous isolines reflect the concentrated DED and the dashed lines indicate the rarefied DED ($\pm 0.05\ e\ Å^{-3}$).

Figure 4 shows the molecular graph for complex **Ia**. It is of interest that this molecular graph has no critical points (3, −1) (CP (3, −1)) or bond paths between the Sb(1) atoms and the carbonyl oxygen atoms (O(2), O(4)). The Sb(1)···O(2) and Sb(1)···O(4) distances are 2.6492(4) and 2.8744(6) Å, which is shorter than the sum of the van der Waals radii of the atoms (3.7 Å [34]). The similar situation is found for other triphenylantimony dicarboxylate complexes [31, 32].

In order to study the structural aspects of the previously detected phase transition (Fig. 1) of triphenylan-

Table 2. Selected bond lengths and topological parameters at the CP (3, −1) for $Ph_3Sb(O_2CC(Me)=CH_2)_2 \cdot C_6H_6$ (**Ia**) according to high-precision X-ray diffraction data

Bond	Distance, Å	ν(**r**), a.u.	ρ(**r**), a.u.	$\nabla^2\rho(\mathbf{r})$, a.u.	$h_e(\mathbf{r})$, a.u.
Sb(1)−O(1)	2.1479(3)	−0.155	0.109	0.151	−0.058
Sb(1)−O(3)	2.1115(3)	−0.173	0.117	0.146	−0.068
Sb(1)···O(2)	2.6492(4)				
Sb(1)···O(4)	2.8744(6)				
Sb(1)−C(9)	2.1106(5)	−0.172	0.122	−0.003	−0.086
Sb(1)−C(15)	2.1185(4)	−0.078	0.064	0.235	−0.010
Sb(1)−C(21)	2.1114(5)	−0.244	0.154	−0.108	−0.135
O(1)−C(1)	1.3064(6)	−0.851	0.339	−1.133	−0.567
O(2)−C(1)	1.2378(7)	−1.109	0.390	−1.022	−0.682
O(3)−C(5)	1.3080(7)	−0.820	0.330	−1.032	−0.539
O(4)−C(5)	1.2370(7)	−1.109	0.390	−1.015	−0.681

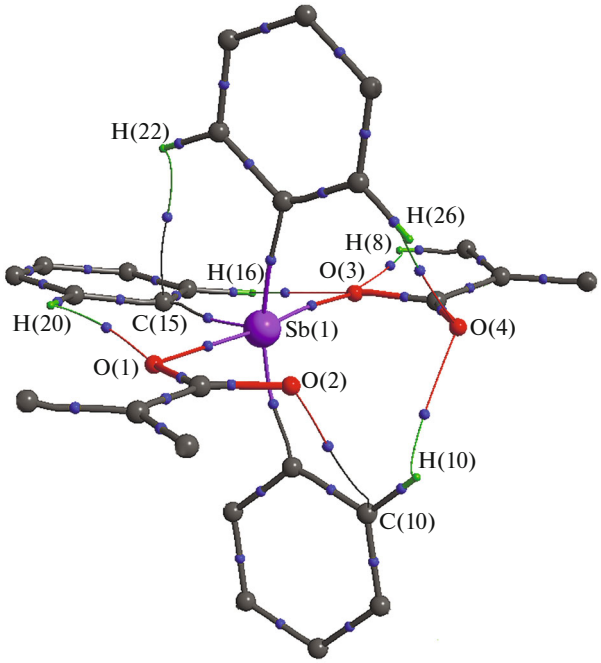

Fig. 4. Experimental molecular graph for $Ph_3Sb(O_2CC(Me)=CH_2)_2$ (**Ia**). The benzene solvation molecule is omitted. Only the CP (3, −1) are presented. The symbols are indicated for atoms involved in the interactions.

timony dimethacrylate [14], we performed X-ray diffraction studies of this compound at temperatures 100 (**Ib**), 145 (**Ic**), 158 (**Id**), and 170 K (**Ie**). Analysis of the geometric characteristics showed that there are no considerable differences between these complexes. In turn, a considerable difference was found between the root-means-square atomic displacements ($\langle u^2 \rangle$) of two chemically equivalent methyl groups at the C(2) and C(6) atoms in the methacrylate ligands (Table 3). As expected (Table 3), the $\langle u^2 \rangle$ values increase in all directions with increasing temperature. However, the root-means-square atomic displacements for the C(4) atom, especially the $\langle u_x^2 \rangle$ values, considerably exceed the typical values. Here it should be noted that the $\langle u^2 \rangle$ values for carbon atoms in the crystals of organic compounds are usually in the 0.015–0.04 Å^2 range (for

Table 3. Root-mean-square atomic displacements of the C(4) and C(8) atoms in **Ib**–**Ie** at various temperatures

Atom	100 K			145 K		
	$\langle u_x^2 \rangle$	$\langle u_y^2 \rangle$	$\langle u_z^2 \rangle$	$\langle u_x^2 \rangle$	$\langle u_y^2 \rangle$	$\langle u_z^2 \rangle$
C(4)	0.0677	0.0375	0.0170	0.0851	0.0507	0.0186
C(8)	0.0394	0.0244	0.0149	0.0506	0.0303	0.0172
	158 K			170 K		
C(4)	0.0898	0.0538	0.0198	0.0960	0.0573	0.0275
C(8)	0.0534	0.0329	0.0186	0.0537	0.0354	0.0258

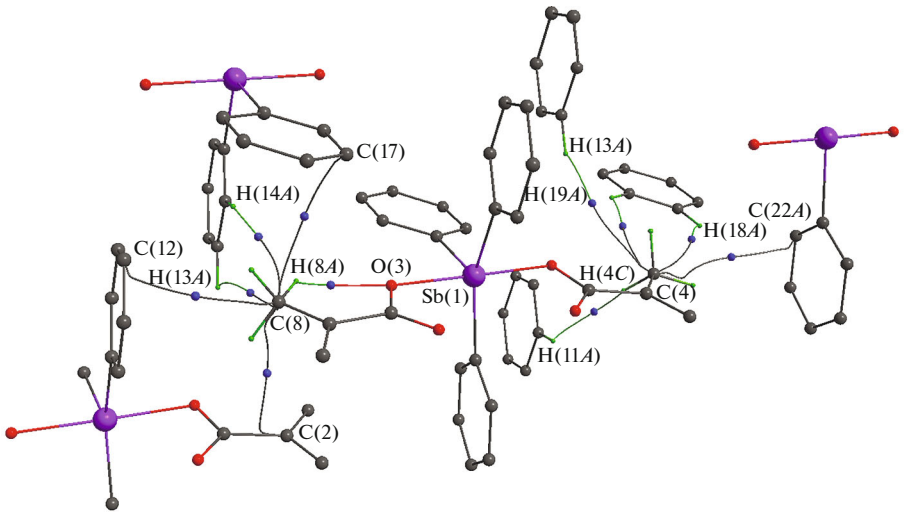

Fig. 5. Fragment of the crystal packing of $Ph_3Sb(O_2CC(Me)=CH_2)_2$ (**Ia**). Only intermolecular bond paths and the CP (3, −1) are shown. The symbols are indicated for atoms involved in the interactions.

100−300 K) [35]. Thus, for the C(4) atom, we observe large librations in the plane perpendicular to the methacrylate moiety (Fig. 2), and these librations are markedly enhanced with temperature rise. Therefore, in our opinion, the phase transition observed in $Ph_3Sb(O_2CC(Me)=CH_2)_2 \cdot C_6H_6$ (**Ib**−**Ie**) is caused by excitation (arrest) of librations of the methyl group at the C(2) atom of the carboxylate ligand. This is consistent with low thermodynamic characteristics of the phase transition ($\Delta_{pt}H^0 = 216.5 \pm 0.4$ J mol^{-1}, $\Delta_{pt}S^0 = 1.370 \pm 0.003$ J mol^{-1} K^{-1}) [14].

In order to interpret these different behaviors of the chemically equivalent Me groups, we identified all intermolecular interactions between the methyl groups at C(2) and C(6) in terms of Bader's theory and estimated their energies using the Espinosa correlation equation [36] (Fig. 5). The methyl group at C(2) has five intermolecular contacts with neighboring molecules, with their energy being −2.1 kcal/mol. In turn, the methyl group at C(6) has four intermolecular and one intramolecular contact. The energy of these contacts is −6.1 kcal/mol. This decreases the root-mean-square atomic displacements of C(8) compared with that of C(4). Here it should be noted that the major contribution to stabilization of the methyl group at C(6) is made by the intramolecular O(3)···H(8*A*) interaction. The energy of this interaction is −2.52 kcal/mol, which is much higher than the energies of the C···C and C···H contacts (−0.25...−0.94 kcal/mol). Thus, higher intermolecular contact energy stabilizes the methyl group at C(6) and decreases its librations as compared with the other Me group. In turn, this leds to smaller volumes of the atomic basins of the $C(8)H_3$ group (29.55 Å^3) in comparison with the $C(4)H_3$ group (33.65 Å^3).

It is noteworthy that in the crystal packing of **Ia**, π···π-interactions occur between the double bonds of the methacrylate moieties of neighboring molecules (Fig. 6). A similar situation is inherent in triphenylantimony diacrylate [32]. However, unlike **Ia**, the complex $Ph_3Sb(O_2CCH=CH_2)_2$ crystallized from benzene contains no solvent molecules. Therefore, we decided to verify whether the packing of complex **Ia** would be retained in the case of crystallization from a non-aromatic solvent (1 : 1 methanol−chloroform or 1 : 1 methanol−THF mixture). All the obtained crystals of **II** had equal unit cell parameters differing from those of complexes **Ia**−**Ie**. An X-ray diffraction study of complex **II** revealed fundamentally different packing motifs (Fig. 7) than those in **Ia**−**Ie**. Hence, the benzene solvate molecule crucially affects the formation of a particular crystal packing in which the phase transition takes place.

Thus, we demonstrated that the phase transition detected in $Ph_3Sb(O_2CC(Me)=CH_2)_2 \cdot C_6H_6$ is caused by excitation (arrest) of librations of the methyl group at the carboxylate C(2) atom. The magnitude of these librations is, in turn, related to the energy of the intra- and intermolecular contacts present in the crystal packing.

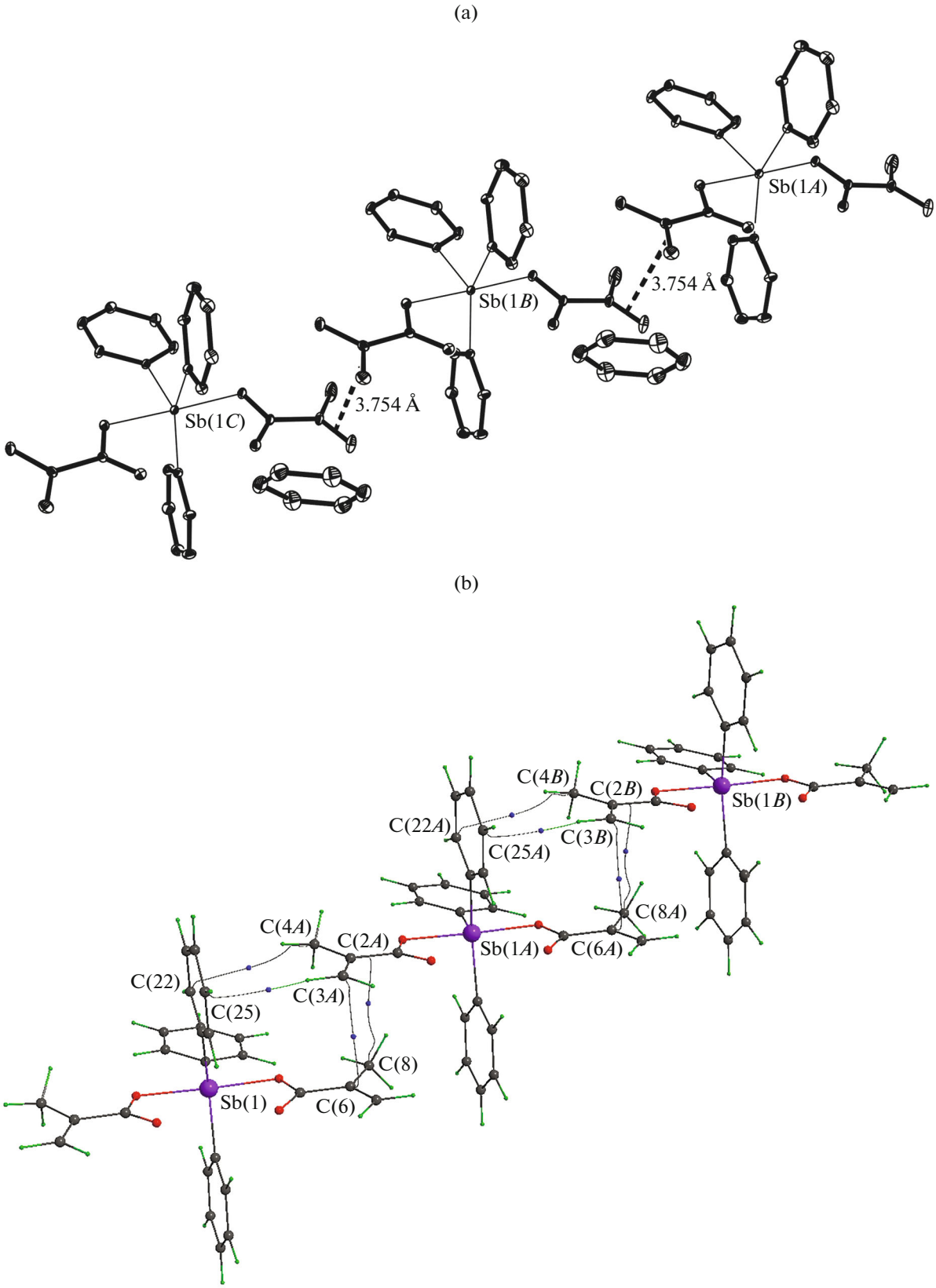

Fig. 6. Fragment of the crystal packing of $Ph_3Sb(O_2CC(Me)=CH_2)_2$ (**Ia**). The benzene solvation molecule is presented in Fig. 6a and is omitted in Fig. 6b. The distances between the midpoints of double bonds are indicated in Fig. 6a. Fig. 6b shows the molecular graph of intermolecular interactions and the corresponding CP (3, −1).

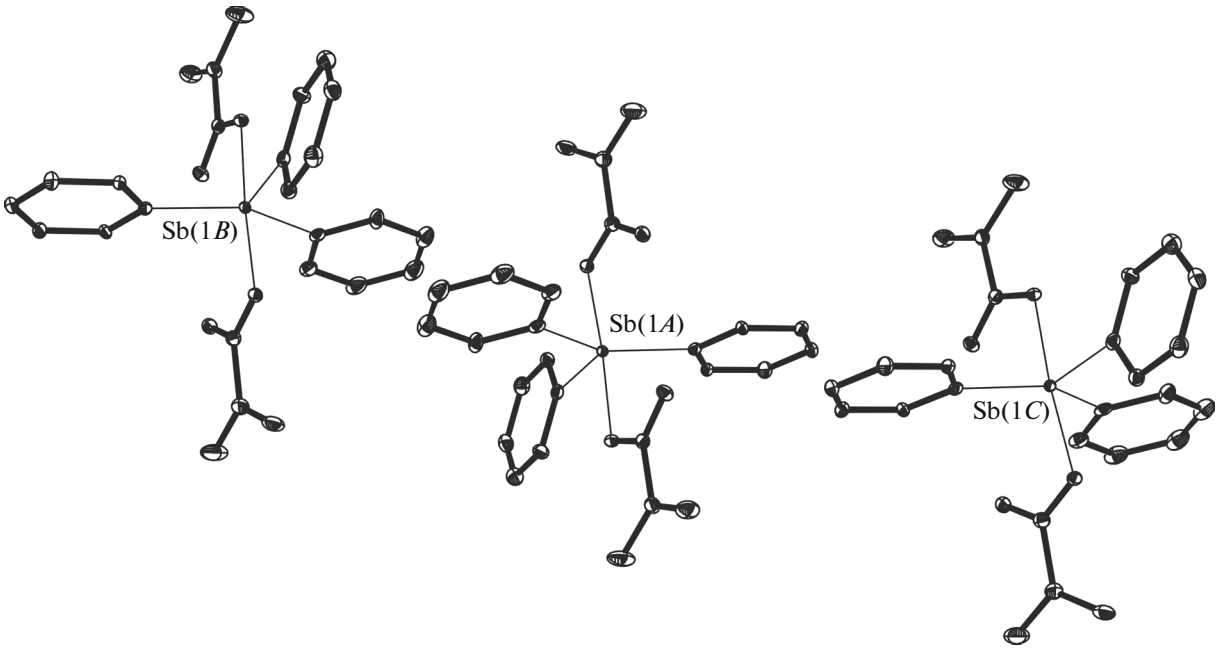

Fig. 7. Fragment of the crystal packing of **II**. The thermal ellipsoids are given at 30% probability level.

ACKNOWLEDGMENTS

This study was supported by the Russian Foundation for Basic Research (project no. 17-03-01257).

REFERENCES

1. Bajpai, K., Singhal, R., and Srivastava, R.C., *Indian J. Chem., Sect. A: Inorg., Bio-Inorg., Phys., Theor. Anal. Chem.*, 1979, vol. 18, p. 73.
2. Singhal, K., Rastogi, R., and Raj, P., *Indian J. Chem., Sect. A: Inorg., Bio-Inorg., Phys., Theor. Anal. Chem.*, 1987, vol. 26, p. 146.
3. Ma, Y., Li, J., Xuan, Z., and Liu, R., *J. Organomet. Chem.*, 2001, vol. 620, nos. 1–2, p. 235.
4. Liu, R.-C., Ma, Y.-Q., Yu, L., et al., *Appl. Organomet. Chem.*, 2003, vol. 17, no. 9, p. 662.
5. Yu, L., Ma, Y.-Q., Liu, R.-C., et al., *Polyhedron*, 2004, vol. 23, no. 5, p. 823.
6. Islam, A., Da Silva, J., Berbet, F., et al., *Molecules*, 2014, vol. 19, no. 5, p. 6009.
7. Islam, A., Rodrigues, B.L., Marzano, I.M., et al., *Eur. J. Med. Chem.*, 2016, vol. 109, p. 254.
8. Qin, W., Yasuike, S., Kakusawa, N., and Kurita, J., *J. Organomet. Chem.*, 2008, vol. 693, no. 17, p. 2949.
9. Gushchin, A.V., Moiseev, D.V., and Dodonov, V.A., *Izv. Akad. Nauk, Ser. Khim.*, 2001, no. 7, p. 1230.
10. Matsukawa, S., Yamamichi, H., Yamamoto, Y., and Ando, K., *J. Am. Chem. Soc.*, 2009, vol. 131, no. 10, p. 3418.
11. Moiseev, D.V., Morugova, V.A., Gushchin, A.V., et al., *J. Organomet. Chem.*, 2004, vol. 689, no. 4, p. 731.
12. Passarelli, J., Murphy, M., Del Re, R., et al., *SPIE Advanced Lithography*, 2015, vol. 9425, p. 94250T-94250T-94213. doi 10.1117/12.2086599
13. Gushchin, A.V., Sharutin, D.V., Prytkova, L.K., et al., *Russ. J. Gen. Chem.*, 2011, vol. 81, no. 3, p. 493.
14. Markin, A.V., Letyanina, I.A., Ruchenin, V.A., et al., *J. Chem. Eng. Data*, 2011, vol. 56, no. 9, p. 3657.
15. Westrum, E.F., Jr. and McCullough, J.P., *Physics and Chemistry of the Organic Solid State*, Fox, M.M.L.D. and Weissberger, A., Eds. New York: Interscience, 1963, vol. 1, p. 1.
16. *SAINT. Data Reduction and Correction Program. Version 8.27B*, Madison: Bruker AXS Inc., 2012.
17. *Data Collection, Reduction and Correction Program. CrysAlis Pro-Software Package*, Agilent Technologies, 2012.
18. Sheldrick G.M., *SADABS-2012/1. Bruker/Siemens Area Detector Absorption Correction Program*, Madison: Bruker AXS Inc., 2012.
19. *SCALE3 ABSPACK: Empirical Absorption Correction. CrysAlis Pro-Software Package*, Agilent Technologies, 2012.
20. Sheldrick, G.M., *SHELXTL. V.6.12. Structure Determination Software Suite*, Madison: Bruker AXS, 2000.
21. Hansen, N.K. and Coppens, P., *Acta Crystallogr., Sect. A: Cryst. Phys., Diffr., Theor. Gen. Crystallogr.*, 1978, vol. 34, no. 6, p. 909.
22. Jelsch, C., Guillot, B., Lagoutte, A., and Lecomte, C., *J. Appl. Crystallogr.*, 2005, vol. 38, no. 1, p. 38.
23. Allen, F.H., Kennard, O., Watson, D.G., et al., *J. Chem. Soc., Perkin Trans.*, 1987, no. 12, p. 2.
24. Hirshfeld, F., *Acta Crystallogr., Sect. A: Cryst. Phys., Diffr., Theor. Gen. Crystallogr.*, 1976, vol. 32, no. 2, p. 239.
25. Stash, A. and Tsirelson, V., *J. Appl. Crystallogr.*, 2002, vol. 35, no. 3, p. 371.

26. Höhne, G.W.H., Hemminger, W.F., and Flammersheim, H.-J., *Differential Scanning Calorimetry*, Heidelberg: Springer, 2003.
27. Drebushchak, V.A., *J. Therm. Anal. Calorim.*, 2005, vol. 79, no. 1, p. 213.
28. Yin, H.-D., Wen, L.-Y., Cui, J.-C., and Li, W.-K., *Polyhedron*, 2009, vol. 28, no. 14, p. 2919.
29. Sharutin, V.V., Sharutina, O.K., Pakusina, A.P., et al., *Russ. J. Inorg. Chem.*, 2008, vol. 53, no. 8, p. 1242.
30. Quan, L., Yin, H.-D., Cui, J.-C., et al., *J. Organomet. Chem.*, 2009, vol. 694, no. 23, p. 3708.
31. Fukin, G.K., Samsonov, M.A., Kalistratova, O.S., and Gushchin, A.V., *Struct. Chem.*, 2016, vol. 27, no. 1, p. 357.
32. Fukin, G.K., Samsonov, M.A., Arapova, A.V., et al., *J. Solid State Chem.*, 2017, vol. 254, p. 32.
33. Bader, R.F.W., *Atoms in Molecules, A Quantum Theory*, Oxford: Oxford Univ., 1990.
34. Batsanov, S., *Zh. Neorg. Khim.*, 1991, vol. 36, no. 12, p. 3015.
35. Trueblood, K.N., *Diffraction Studies of Molecular Motions in Crystals*, Oxford: Oxford Univ., 1992, p. 199.
36. Espinosa, E., Molins, E., and Lecomte, C., *Chem. Phys. Lett.*, 1998, vol. 285, nos. 3–4, p. 170.

Translated by Z. Svitanko